CrystEngComm

ROYAL SOCIETY OF CHEMISTRY

PAPER

View Article Online
View Journal | View Issue

Cite this: *CrystEngComm*, 2022, **24**, 6747

In situ time-resolved monitoring of mixed-ligand metal–organic framework mechanosynthesis†

Max Rautenberg,[ab] Biswajit Bhattacharya,*[a] Julia Witt,[a] Mohit Jain[ac] and Franziska Emmerling*[ab]

Received 10th June 2022,
Accepted 4th September 2022

DOI: 10.1039/d2ce00803c

rsc.li/crystengcomm

The mechanism of mixed-ligand metal–organic framework (MOF) formation, and the possible role of intermediate single-ligand metal complexes during mechanosynthesis, have not been explored yet. For the first time, we report here *in situ* real-time monitoring of the mechanochemical formation mechanism of mixed-ligand MOFs. Our results show that binary phases can act as intermediates or competing products in one-pot and stepwise synthesis.

Metal–organic frameworks (MOFs) are crystalline porous materials built from inorganic metal nodes connected with organic ligands resulting in two- or three-dimensional network structures with potential voids.[1,2] Thanks to their inherent porosity and large surface area, these materials are ideal candidates in gas storage/separation,[3,4] sensing,[5,6] and catalysis.[7] The unique combination of compositional modularity of MOFs by varying the organic/inorganic subunit has further propelled research interest in these materials.[8,9] In this regard, mixed-ligand approaches comprising two different types of ligands with distinct functionalities, such as carboxylate or phosphonate groups combined with a basic N, N′-donor ligand, were introduced as a successful strategy for tuning the physicochemical properties of MOFs.[10–12] Despite several advancements, the development of new MOF materials is still typically based on trial-and-error. The investigation of the reaction parameters such as concentration, time, temperature, or solvent conditions required for a desired MOF structure is demanding and needs combinatorial screening. Recently, different spectroscopic and computational approaches have been used to study the crystal nucleation and growth of MOFs.[13–16] However, there is still a lack of understanding of the formation mechanism, *i.e.*, how chemical coordination between metal nodes and organic ligands occurs during MOF self-assembly or which fundamental building units govern the MOF synthesis.

In this regard, environmentally benign rapid mechanochemical syntheses provide an opportunity to study the real-time chemical transformations of a wide range of solid molecules and materials including nanomaterials, alloys, organometallic complexes, pharmaceutical cocrystals, and MOFs.[17–25] Mechanochemical grinding or milling of solids performed either under solvent-free conditions or using catalytic amounts of solvent can easily be monitored by time-resolved *in situ* (TRIS) X-ray diffraction or spectroscopy probing the local geometry, phase composition, and crystallinity of intermediates and products.[26–30] TRIS X-ray powder diffraction,[31–33] Raman spectroscopy,[28] and thermography[30] or combinations thereof[34,35] provided insights into the mechanism of mechanochemical syntheses of MOFs. Very recently, our group demonstrated the accurate measurement of the microstructure of ZIF-8 during ball milling by introducing a new kind of milling jar in time-resolved *in situ*-XRD measurements.[36] Typically, investigations are focused on the synthesis of single ligand MOFs and examples of mixed-ligand MOFs are scarce. The competitive coordination of the metal ions by two different ligands allows to tune the network structures in mixed-ligand MOFs. Different possibilities for the formation of single-component coordination complexes exist along with dual ligand complexes. The question arises as to what role the individual coordination complexes play in the formation of the MOFs with mixed ligands. Thus, the formation mechanism of these materials must be better understood before such materials can be selectively prepared in bulk scale for targeted practical applications.

In this work, we explored the mechanochemical synthesis of two isostructural mixed ligand phosphonate-based proton conductive MOFs,[37] $\{Co(H_2PhDPA)(4,4'\text{-bipy})(H_2O)\cdot 2H_2O\}_n$ (BAM-1), $\{Fe(H_2PhDPA)(4,4'\text{-bipy})(H_2O)\cdot 2H_2O\}_n$ (BAM-2) [where H_2PhDPA^{2-} = phenylenediphosphonate and 4,4′-bipy =

[a] *BAM Federal Institute for Materials Research and Testing, Richard-Willstätter-Str. 11, 12489 Berlin, Germany. E-mail: franziska.emmerling@bam.de*
[b] *Department of Chemistry, Humboldt-Universität zu Berlin, Brook-Taylor-Str. 2, 12489 Berlin, Germany*
[c] *Department of Materials Science, Technical University of Darmstadt, Karolinenplatz 5, 64289 Darmstadt, Germany*

† Electronic supplementary information (ESI) available: Time-resolved *in situ* XRD data, Raman data and electrochemical measurements. See DOI: https://doi.org/10.1039/d2ce00803c

4,4′-bipyridine] by using tandem real-time *in situ* powder X-ray diffraction (PXRD). Along with the one-pot synthesis, the step-by-step reactions where the metal source reacts with one ligand first and subsequently with the second ligand are monitored to extract detailed information on the development of the product structure. The insight gained from these incremental and one-pot syntheses allows us to estimate formation mechanisms for BAM-1 and BAM-2.

Liquid assisted grinding (LAG) of a stoichiometric mixture of $Co(OAc)_2{\cdot}4H_2O$ or $FeCl_2{\cdot}4H_2O$ and $NaHCO_3$ with 4,4′-bipy and H_4PhDPA at 50 Hz for 30 min led to the formation of BAM-1 and BAM-2 (Fig. 1). BAM-1 was obtained as a pure phase, whereas the formation of BAM-2 was not completed even after prolong grinding. A washing step with water was needed to remove the side products from the obtained powder of BAM-2.

The formation mechanism of phosphonate based mixed-ligand MOFs could in principle follow different pathways: i) the metal precursor can react with one of the organic linkers to form a single ligand-based metal complex, which further reacts with the second linker to form the final framework. ii) Alternatively, the simultaneous coordination of both ligands to the metal centre is also a plausible mechanism. To understand which pathway leads to the final MOF and which is favoured, we split the mechanochemical synthesis of BAM-1 and BAM-2 into two two-step reactions, consisting of one ligand offered in each step. The synthesis increments and the one-pot reactions are monitored by *in situ* PXRD to assess the conversion and formation rates of the reactions and the possible mechanisms.

During the three-component reaction of BAM-1, the early stage of the transformation shows a loss of intensity of the diffraction of starting materials. This could be attributed to an amorphization of the starting materials or the powder getting stuck in the milling vessel. The sudden appearance of reflections at q = 9.1 nm^{-1} for 15 s and q = 14.3 nm^{-1} for 10 s suggests that crystalline material is present but does not pass through the beam. After 1 min of milling, reflections of BAM-1 start to grow, and reach a plateau after approximately 2 min (Fig. 2a and S1†). For BAM-2, Bragg reflections from starting materials disappear after 30 s and new reflections grow in the early stage of the reaction. These new reflections (q = 7.61, 10.53, 17.28 nm^{-1}) are consistent with a mixture of $FeCl_2$(4,4′-bipy) and unidentified phases. With continued milling, the reflections of BAM-2 appear. After 30 min of grinding the reflections of BAM-2 reach the maximum

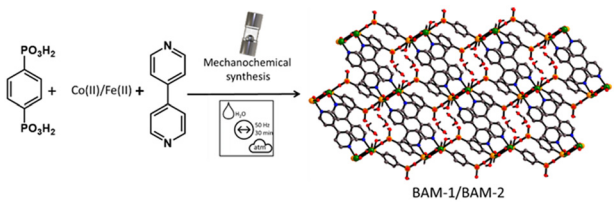

Fig. 1 Schematic presentation of the mechanochemical synthesis of BAM-1 and BAM-2 by ball milling.

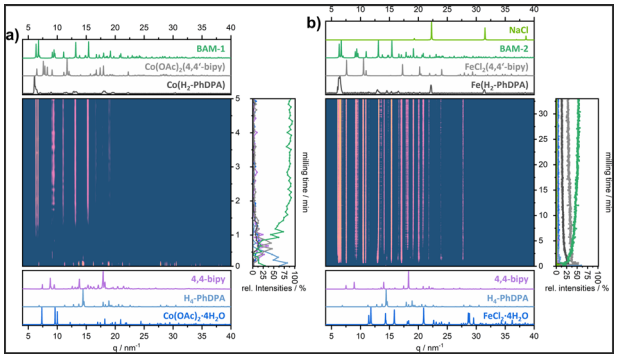

Fig. 2 TRIS XRD pattern of the mechanochemical one-pot reactions of BAM-1 (a) and BAM-2 (b).

intensity, leading to a mixture of BAM-2, $FeCl_2$(4,4′-bipy)[38] and an unknown phase, that persist even after 10 h of extensive grinding (Fig. 2b and S2†).

The three-component reactions showed a difference for the two metal atoms (M = Co, Fe). Specifically, the formation of BAM-2 passed through a binary phase intermediate in contrast to BAM-1. We therefore aim to better understand if the difference in reaction pathways relates to the existence of binary phases of both metal complexes, the relative reactivity of the binary phases, or relative kinetics of their formation.

To probe this, we have conducted step by step reactions where the ligands are added sequentially in the reaction vessel (Scheme 1). The TRIS XRD data for milling 4,4′-bipy with $Co(OAc)_2{\cdot}4H_2O$ or $FeCl_2{\cdot}4H_2O$ (Scheme 1, reactions Ia) show a rapid consumption of the starting material, leading to the formation of $\{Co(OAc)_2(4,4'\text{-bipy})\}_n$ (ref. 39) or $\{FeCl_2(4,4'\text{-bipy})\}_n$, respectively. Both reactions were completed within 4 min and 30 s for Co(II) and Fe(II), and no further changes were observed within 30 min of grinding (Fig. 3a and e and S3 and S4†). The subsequent addition of H_4-PhDPA (Scheme 1, reactions Ib) led to the conversion of $\{Co(OAc)_2(4,4'\text{-bipy})\}_n$ to BAM-1, which was completed after 3 min of grinding (Fig. 3b, and S5†). Whereas, during milling of $\{FeCl_2(4,4'\text{-bipy})\}_n$ with H_4-PhDPA and $NaHCO_3$, BAM-2 starts to grow with simultaneous consumption of $\{FeCl_2(4,4'\text{-bipy})\}_n$ (Fig. 3f and S6†). After 35 min of grinding,

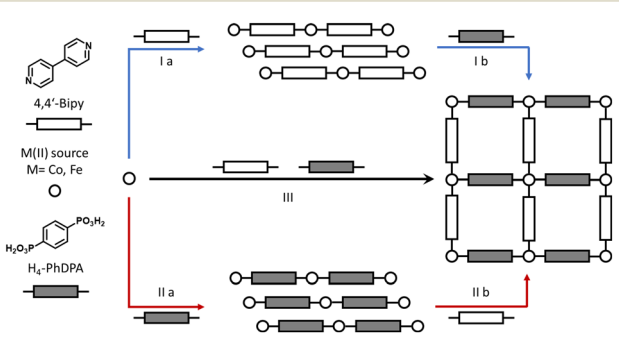

Scheme 1 Three synthesis pathways towards BAM-1 and BAM-2 either as incremental approaches (top, blue, Ia and Ib; or bottom, red IIa and IIb) or direct one-pot approach (middle, black, III).

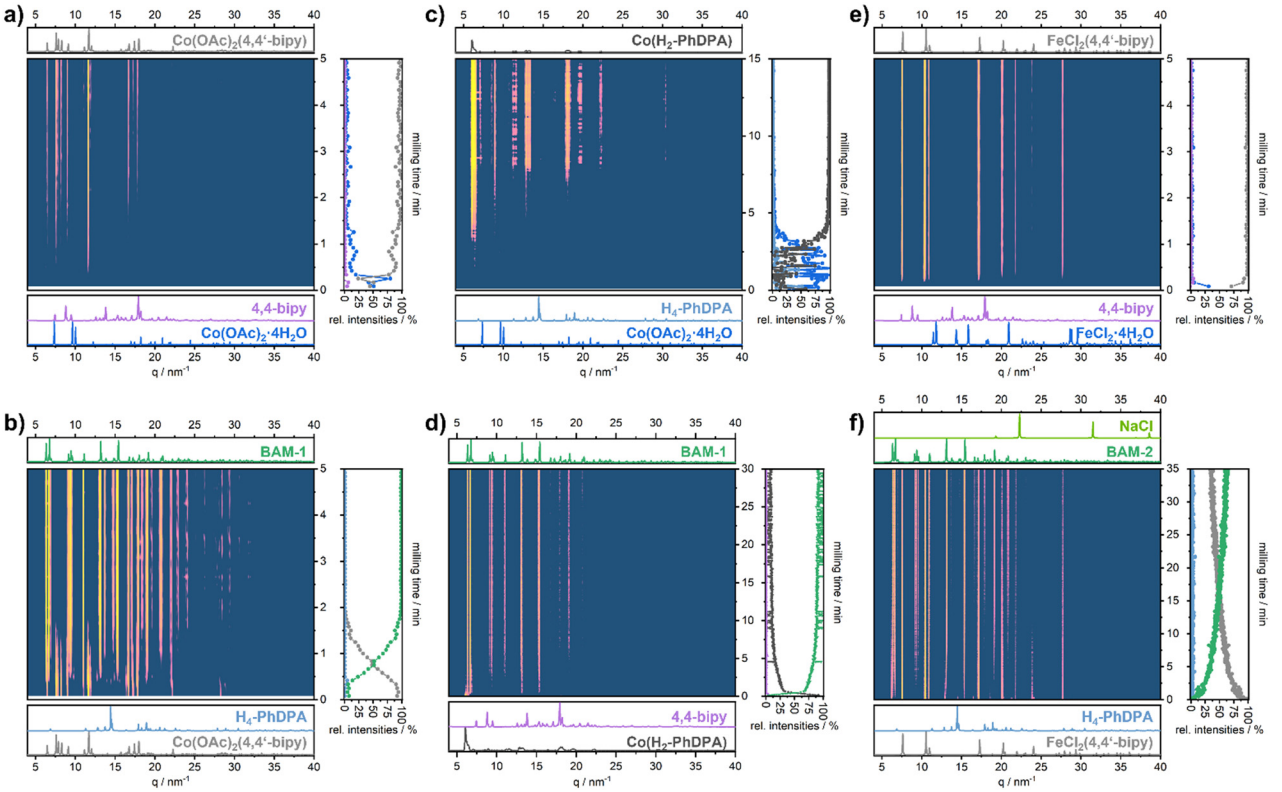

Fig. 3 TRIS PXRD data of the mechanochemical reactions Ia (a), Ib (b), IIa (c), and IIb (d) for BAM-1 and reactions Ia (e) and Ib (f) for BAM-2 (see Scheme 1 for reaction overview).

approximately 65% conversion to BAM-2 was observed. The incomplete conversion to BAM-2 is consistent with the one-pot synthesis, see Fig. 2b and S2.†

Initially, no crystalline phases were detected in the experiments reversing the order of ligand addition milling $Co(OAc)_2{\cdot}4H_2O$ with H_4-PhDPA (Scheme 1, reactions IIa, Fig. 3c and S7†). Reflections appear around 4 min and continue to grow, reaching a plateau at 8 min. The reflections could not be assigned to any known crystalline phase, but it can be assumed that mixtures of cobalt–phenylenediphosphonates (*e.g.* $Co(H_2$-PhDPA)) with varying stoichiometry are present (Fig. 3b and S7†). With the addition of 4,4′-bipy (Scheme 1, reactions IIb), the presumed mixture of $Co(H_2PhDPA)$ is consumed within the first minute of milling (Fig. 3d and S9†). Finally, the crystallization of BAM-1 starts and continues over the next 14 min. In contrast, co-grinding $FeCl_2{\cdot}4H_2O$ with H_4-PhDPA, and $NaHCO_3$, yielded reflections of the side product NaCl and another unknow crystalline phase, presumably $Fe(H_2$-PhDPA) (Fig. S8†). We suspect that this is the same unknown phase as observed in the one pot synthesis. Surprisingly, milling this unknown phase with 4,4′-bipy (IIb), did not yield BAM-2, but a complete consumption of NaCl and a partial consumption of 4,4′-bipy can be observed. This can be explained by the formation of a 4,4′-bipy-hydrogen chloride salt or a hydrate thereof (Fig. S10†).

Moreover, we have tested the bulk synthesized BAM-1 and BAM-2 as electrocatalysts for water splitting (see ESI:† Fig. S17). Both compounds exhibit moderate reactivity towards oxygen evolution reaction (OER), which need further investigations for a follow-up work.

Our stepwise synthesis demonstrates that the binary phases can in principle behave as intermediates for the formation of BAM-1. Their absence in the one-pot synthesis can be ascribed to their rapid consumption, consistent to the speed of their reactivity during step-wise synthesis. However, we have shown that BAM-2 can only form *via* a single step reaction or the binary phase, $\{FeCl_2(4,4'\text{-bipy})\}_n$. The binary phase $Fe(H_2$-PhDPA) is instead a competitive product, and its formation is responsible for the inability to achieve the quantitative yield of BAM-2 during the one-pot synthesis. Our studies reveal the complex behaviour of mechanochemical synthesis of mixed ligand metal organic frameworks. We expect further investigation in these directions will provide exciting insights into the mechanisms of materials synthesis by environmentally benign ways.

Conflicts of interest

There are no conflicts to declare.

Acknowledgements

We thank the Helmholtz-Zentrum Berlin für Materialien und Energie for the allocation of synchrotron radiation beamtime.

Gefördert durch die Deutsche Forschungsgemeinschaft (DFG) – Projektnummer 387284271 – SFB 1349. Funded by the Deutsche Forschungsgemeinschaft (DFG, German Research Foundation) – Project-ID 387284271 – SFB 1349.

Notes and references

1 S. R. Batten, N. R. Champness, X.-M. Chen, J. Garcia-Martinez, S. Kitagawa, L. Öhrström, M. O'Keeffe, M. Paik Suh and J. Reedijk, *Pure Appl. Chem.*, 2013, **85**, 1715–1724.
2 M. Eddaoudi, J. Kim, N. Rosi, D. Vodak, J. Wachter, M. O'Keeffe and O. M. Yaghi, *Science*, 2002, **295**, 469–472.
3 R.-B. Lin, S. Xiang, W. Zhou and B. Chen, *Chem*, 2020, **6**, 337–363.
4 K.-J. Chen, D. G. Madden, S. Mukherjee, T. Pham, K. A. Forrest, A. Kumar, B. Space, J. Kong, Q.-Y. Zhang and M. J. Zaworotko, *Science*, 2019, **366**, 241–246.
5 B. Bhattacharya, A. Halder, L. Paul, S. Chakrabarti and D. Ghoshal, *Chem. – Eur. J.*, 2016, **22**, 14998–15005.
6 E. A. Dolgopolova, A. M. Rice, C. R. Martin and N. B. Shustova, *Chem. Soc. Rev.*, 2018, **47**, 4710–4728.
7 A. Bavykina, N. Kolobov, I. S. Khan, J. A. Bau, A. Ramirez and J. Gascon, *Chem. Rev.*, 2020, **120**, 8468–8535.
8 E. A. Dolgopolova, O. A. Ejegbavwo, C. R. Martin, M. D. Smith, W. Setyawan, S. G. Karakalos, C. H. Henager, H.-C. zur Loye and N. B. Shustova, *J. Am. Chem. Soc.*, 2017, **139**, 16852–16861.
9 J. B. Bailey, L. Zhang, J. A. Chiong, S. Ahn and F. A. Tezcan, *J. Am. Chem. Soc.*, 2017, **139**, 8160–8166.
10 B. Bhattacharya and D. Ghoshal, *CrystEngComm*, 2015, **17**, 8388–8413.
11 S. Pullen and G. H. Clever, *Acc. Chem. Res.*, 2018, **51**, 3052–3064.
12 M. Du, C.-P. Li, C.-S. Liu and S.-M. Fang, *Coord. Chem. Rev.*, 2013, **257**, 1282–1305.
13 M. J. Van Vleet, T. Weng, X. Li and J. R. Schmidt, *Chem. Rev.*, 2018, **118**, 3681–3721.
14 T. D. Petersen, G. Balakrishnan and C. L. Weeks, *Dalton Trans.*, 2015, **44**, 12824–12831.
15 S. Hermes, T. Witte, T. Hikov, D. Zacher, S. Bahnmüller, G. Langstein, K. Huber and R. A. Fischer, *J. Am. Chem. Soc.*, 2007, **129**, 5324–5325.
16 F. Millange, M. I. Medina, N. Guillou, G. Férey, K. M. Golden and R. I. Walton, *Angew. Chem., Int. Ed.*, 2010, **49**, 763–766.
17 A. A. L. Michalchuk, E. V. Boldyreva, A. M. Belenguer, F. Emmerling and V. V. Boldyrev, *Front. Chem.*, 2021, **9**, 685789.
18 T. Stolar and K. Užarević, *CrystEngComm*, 2020, **22**, 4511–4525.
19 L. Tröbs and F. Emmerling, *Faraday Discuss.*, 2014, **170**, 109–119.
20 V. Shivam, J. Basu, Y. Shadangi, M. K. Singh and N. K. Mukhopadhyay, *J. Alloys Compd.*, 2018, **757**, 87–97.
21 P. F. M. de Oliveira, A. A. L. Michalchuk, A. G. Buzanich, R. Bienert, R. M. Torresi, P. H. C. Camargo and F. Emmerling, *Chem. Commun.*, 2020, **56**, 10329–10332.
22 H. Kulla, A. A. L. Michalchuk and F. Emmerling, *Chem. Commun.*, 2019, **55**, 9793–9796.
23 M. Klimakow, P. Klobes, A. F. Thunemann, K. Rademann and F. Emmerling, *Chem. Mater.*, 2010, **22**, 5216–5221.
24 A. L. Garay, A. Pichon and S. L. James, *Chem. Soc. Rev.*, 2007, **36**, 846–855.
25 A. Pichon, A. Lazuen-Garay and S. L. James, *CrystEngComm*, 2006, **8**, 211–214.
26 T. Friščić, I. Halasz, P. J. Beldon, A. M. Belenguer, F. Adams, S. A. J. Kimber, V. Honkimäki and R. E. Dinnebier, *Nat. Chem.*, 2013, **5**, 66–73.
27 A. A. L. Michalchuk and F. Emmerling, *Angew. Chem., Int. Ed.*, 2022, **61**(21), e202117270.
28 S. Lukin, K. Užarević and I. Halasz, *Nat. Protoc.*, 2021, **16**, 3492–3521.
29 I. Sović, S. Lukin, E. Meštrović, I. Halasz, A. Porcheddu, F. Delogu, P. C. Ricci, F. Caron, T. Perilli, A. Dogan and E. Colacino, *ACS Omega*, 2020, **5**, 28663–28672.
30 H. Kulla, M. Wilke, F. Fischer, M. Röllig, C. Maierhofer and F. Emmerling, *Chem. Commun.*, 2017, **53**, 1664–1667.
31 T. Stolar, L. Batzdorf, S. Lukin, D. Žilić, C. Motillo, T. Friščić, F. Emmerling, I. Halasz and K. Užarević, *Inorg. Chem.*, 2017, **56**, 6599–6608.
32 L. S. Germann, A. D. Katsenis, I. Huskić, P. A. Julien, K. Užarević, M. Etter, O. K. Farha, T. Friščić and R. E. Dinnebier, *Cryst. Growth Des.*, 2020, **20**, 49–54.
33 J. Beamish-Cook, K. Shankland, C. A. Murray and P. Vaqueiro, *Cryst. Growth Des.*, 2021, **21**, 3047–3055.
34 L. Batzdorf, F. Fischer, M. Wilke, K.-J. Wenzel and F. Emmerling, *Angew. Chem.*, 2015, **127**, 1819–1822.
35 H. Kulla, S. Haferkamp, I. Akhmetova, M. Röllig, C. Maierhofer, K. Rademann and F. Emmerling, *Angew. Chem., Int. Ed.*, 2018, **57**, 5930–5933.
36 G. I. Lampronti, A. A. L. Michalchuk, P. P. Mazzeo, A. M. Belenguer, J. K. M. Sanders, A. Bacchi and F. Emmerling, *Nat. Commun.*, 2021, **12**, 6134.
37 M. Rautenberg, B. Bhattacharya, C. Das and F. Emmerling, *Inorg. Chem.*, 2022, **61**, 10801–10809.
38 M. A. Lawandy, X. Huang, R.-J. Wang, J. Li, J. Y. Lu, T. Yuen and C. L. Lin, *Inorg. Chem.*, 1999, **38**, 5410–5414.
39 J. Lu, C. Yu, T. Niu, T. Paliwala, G. Crisci, F. Somosa and A. J. Jacobson, *Inorg. Chem.*, 1998, **37**, 4637–4640.

